Crystal structure and hydrogenation properties of pseudo-binary $Mg_6Pd_{0.5}Ni_{0.5}$ complex metallic alloy

F. Cuevas [a,*], J.F. Fernández [b], J.R. Ares [b], F. Leardini [b], M. Latroche [a]

[a] CMTR/ICMPE/CNRS, 2-8 rue Henri Dunant, 94320 Thiais Cedex, France
[b] Dpto. Física de Materiales, Facultad de Ciencias, Universidad Autónoma de Madrid, 28049 Madrid, Spain

ARTICLE INFO

ABSTRACT

The crystal structure of the Ni-substituted $Mg_{6.10(2)}Pd_{0.52(2)}Ni_{0.41(2)}$ complex metallic alloy has been determined by X-ray and neutron powder diffraction. The reaction of this compound at 573 K towards deuterium absorption for pressures up to 23 bar has also been studied. The crystal structure of $Mg_{6.10(2)}Pd_{0.52(2)}Ni_{0.41(2)}$ compound was determined in the light of Samson's [Acta Crystallogr. B 28 (1972) 936] and Makongo's (Philos. Mag. 86 (2006) 427] models for the binary Mg_6Pd compound. It crystallizes in $F\bar{4}3m$ space group with lattice parameter 20.13331(7) Å. The refined unit-cell composition is $Mg_{342(1)}Pd_{29(1)}Ni_{23(1)}$ with $Z = 56$. Nickel by palladium substitution is not fully random. Nickel atoms preferentially locate on Pd sites with low coordination number due to steric effects. Deuterium uptake is 9.6 D/f.u. under the given conditions of pressure and temperature. Upon absorption, the intermetallic compound disproportionates into MgD_2, Mg_5Pd_2 and Mg_2NiD_4 phases. The Mg_2NiD_4 phase is observed to crystallize in the orthorhombic LT2 modification for which an averaged crystal structure in the $Pcc2$ space group is proposed.

© 2009 Elsevier Inc. All rights reserved.

1. Introduction

Magnesium metal is one of the most interesting materials for solid hydrogen storage. Its hydride, MgH_2, has both high specific and volumetric hydrogen content: 7.6 wt% H and $108\,g_{H_2}/l$, respectively. Magnesium hydride is, however, too stable for room temperature (RT) applications ($\Delta H_f^\circ = -75$ kJ/mol H_2). To reach atmospheric pressure, the Mg/MgH_2 system has to be heated up to 560 K [1].

MgH_2 can be destabilized by magnesium alloying with transition metals. For instance, Mg_2Ni forms a hydride Mg_2NiH_4 and the atmospheric pressure is obtained at a lower temperature (526 K) [2]. This improvement is counterbalanced by the fact that the specific hydrogen content decreases to 3.6 wt% H. Such a reduction can be linked to the lower capability of the transition metal to store hydrogen. Mg absorbs two hydrogen atoms per metal atom (H/M), whereas Ni only absorbs 1 H/M and this at very high pressures [3].

Recently, much attention has been devoted to the properties of Mg_6Pd complex metallic alloy as hydrogen storage material [4–8]. Pd metal is known to have prominent properties for hydrogen dissociation and forms a reversible hydride, $PdH_{0.7}$, under normal conditions of pressure and temperature [9]. Furthermore, since the atomic Pd:Mg ratio in Mg_6Pd compound is low, 14 at%, the hydrogen capacity is expected to remain high. Several authors have reported that the hydrogenation of Mg_6Pd compound is reversible and occurs through three disproportion reactions with a global hydrogen uptake about 4 wt% H [7,8]. The fully hydrided state leads to the formation of a mixture of MgPd and MgH_2 phases.

We have started a research study on the feasibility of partial substitution of Pd by Ni in Mg_6Pd compound and its effects on its hydrogenation reaction. Pd and Ni have the same electronic outer shell configuration and, therefore, possess close chemical properties. This is reflected by their complete miscibility as observed in the binary Pd–Ni phase diagram. However, published data on the ternary Mg–Ni–Pd phase diagram at 673 K indicate that the Ni substitution in Mg_6Pd phase to form pseudo-binary $Mg_6Pd_{1-x}Ni_x$ compounds is very limited ($\sim$3 wt%, i.e. $x\sim$0.13) [10]. This result is rather striking, especially after taking into consideration the crystal structure and phase stability of Mg_6Pd and Mg_6Ni compounds. Mg_6Pd compound is thermodynamically stable. It crystallizes in the cubic $F\bar{4}3m$ space group with lattice parameter 20.182 Å [11]. As for Mg_6Ni, it can be obtained as a metastable phase either by thermal annealing at $\sim$ 475 K of melt-spun ribbons [12,13] or by high-pressure synthesis [14]. Interestingly, metastable Mg_6Ni is isostructural to Mg_6Pd with lattice parameter 19.987 Å [14]. This suggests that $Mg_6Pd_{1-x}Ni_x$ compounds might be obtained as stable phases at higher Ni contents than previously reported. As a matter of fact, we have recently succeeded in the

elaboration of thermodynamically stable $Mg_6Pd_{0.5}Ni_{0.5}$ compound [15]. The determination of the crystal structure of the pseudo-binary $Mg_6Pd_{0.5}Ni_{0.5}$ compound and its behavior towards hydrogen absorption is the scope of this paper.

2. Experimental

An alloy ingot 50 g in mass with nominal composition $Mg_6Pd_{0.5}Ni_{0.5}$ was prepared by induction melting under argon followed by casting. To minimize Mg losses due to volatilization, a Mg–Ni pre-alloy close to the eutectic composition of 89 at% Mg was first elaborated. Then, elemental Pd and Mg were added to the pre-alloy before the final melting. The purity of the metal constituents was 99.8% for Mg and better than 99.9% for Pd and Ni. To ensure chemical homogeneity, 10 g of this alloy was annealed in a silica tube at 660 K in 1 bar of argon for 72 h. Sample cooling was achieved by removing the silica tube from the furnace.

Alloy composition was analyzed by electron probe micro-analysis (EPMA) in a Cameca SX-100 instrument operated at 15 kV. Alloy bulk density was measured with a helium pycn-ometer (Micrometrics Accupyc 1330). Its crystal structure was studied at room temperature both by X-ray and neutron powder diffraction (XRPD and NPD, respectively). For XRPD measure-ments, 0.5 g of alloy were grinded and sieved down to 63 μm. XRPD measurements were performed with a θ–θ diffractometer (Bruker AXS D8Advance equipped with backscattered rear graphite monochromator) using Cu$K\alpha$ radiation. The intensity of the diffraction peaks for XRPD data was observed to slightly depend on the specimen preparation, much probably due to preferential orientation. Therefore XRPD data for the alloy was only used for indexation purposes. As for NPD measurements, 5 g of the alloy ingot were grinded in an agate mortar under argon atmosphere, sieved down to 125 μm, and placed into a vanadium tube. NPD experiments were performed on the 3T2 high resolution beam-line at LLB Saclay, France. The data were recorded over the range 4.4–122° by steps of 0.05° at a wavelength of $\lambda = 1.2243$ Å.

After NPD measurements, the alloy was deuterated in a Sievert's type apparatus. Its pressure–composition isotherm for deuterium absorption was obtained at 573 K using deuterium pressures up to 23 bar. Next, the sample was cooled down to room temperature under deuterium pressure (cooling time ∼6 h, P_{D_2}∼20 bar). Part of the sample (∼4.5 g) was then transferred into a vanadium tube under argon atmosphere and its crystal structure was studied by NPD. The rest (∼0.5 g) was used for XRPD measurements. For the deuterated sample, joint XRPD and NPD Rietveld analysis were performed. All diffraction data were analyzed by the Rietveld method using the Fullprof software [16]. The used scattering amplitudes ($\times 10^{-12}$ cm) for neutron diffraction are $b_{Mg} = 0.537$, $b_{Pd} = 0.591$ and $b_{Ni} = 1.036$.

3. Results and discussion

3.1. Composition and crystal structure determination of $Mg_6Pd_{0.5}Ni_{0.5}$ compound

EPMA analysis performed on hundred randomly distributed points of the alloy showed that it was single-phase with atomic composition $Mg_{86.7(2)}Pd_{7.4(2)}Ni_{5.9(3)}$. The alloy bulk density was measured to be 2.58(1) g/cm³. All diffraction peaks observed in the XRPD and NPD patterns could be indexed in the cubic $F\bar{4}3m$ space group with lattice parameter 20.13331(7) Å. The Mg_6Pd phase is reported by Makongo et al. to exist within a wide range of

homogeneity that extends from 85.0 to 87.4 at% Mg leading to a variation in the cubic lattice parameter from 20.045 to 20.196 Å [17]. Therefore, the chemical composition of the here synthesized compound is expected to be close to the Mg-rich limit.

The NPD data were analyzed by the Rietveld method. As a first approach, the structural model proposed by Samson et al. for the Mg_6Pd compound was used but allowing for partial occupation of Ni atoms in Pd sites (i.e. atom nos. 10, 11, 12 and 13 in Ref. [11]). In this model, one should take into consideration that site 12 can simultaneously be occupied by Mg, Ni and Pd atoms, which prevents determining the fractional atomic occupancy on this site from a unique set of data. Nevertheless, the refinement of the overall scattering amplitude from this site is very low ($b_{12} = 0.53 \times 10^{-12}$ cm), which points to a minor Ni occupancy. Assuming no occupancy of Ni on this site, the refinement converges rapidly to get low residuals $R_B = 2.42\%$ and $R_{wp} = 1.88\%$, though the isotropic displacement factor of site 12 was found to be excessively high 3.1 Å².

To get a more reasonable structural refinement, we checked the structural model proposed by Makongo et al. at the Mg-rich limit of the Mg_6Pd phase [17]. At this limit, an additional site for Mg atoms, hereafter labeled as site 12b, is proposed. Mg occupancy on site 12b coincides with vacancies on sites 12 (hereafter labeled as site 12a) and 14. In other words, when a Mg vacancy is created at site 14, the atom located at site 12a shrinks towards site Mg14 at the center of the polyhedron to occupy the additional 12b site. This latter site is located along the line that links site 12a to site 14 (see Fig. 1). Therefore, as regards the site occupancy factors (SOF) of sites 12a, 12b and 14, this model provides two crystallographic constraints: (i) Σ (SOF12a, SOF 12b) = 1 and (ii) Σ (SOF12b, SOF14) = 1. Moreover, according to Makongo's model, site 12b is exclusively occupied by Mg. This fact can be understood in terms of the large free-volume available at site 12b due to vacancies on neighboring sites 12a and 14. Thus, site 12b can easily accommodate Mg despite its larger metallic radius ($r_{Mg} = 1.60$ Å, $r_{Pd} = 1.37$ Å). Using this model and keeping no occupancy of Ni on site 12a, the isotropic displacement factor of site 12a decreased to 1.3 Å² and residuals also decreased to $R_B = 2.04\%$ and $R_{wp} = 1.76\%$.

Finally, the site occupancy factor for each element M at site 12a (SOF$_M$12a, with M = Mg, Ni, Pd) was determined by the help of analytical relationships using chemical and crystallographic constraints. As a matter of fact, three independent equations are needed to establish the three variables, i.e. the three SOF$_M$12a values. Two of them were obtained by equalizing the quotient Σ (amount of M atoms)/Σ (total amount of atoms) in the unit-cell to the result of EPMA analysis for two out of the three M atoms

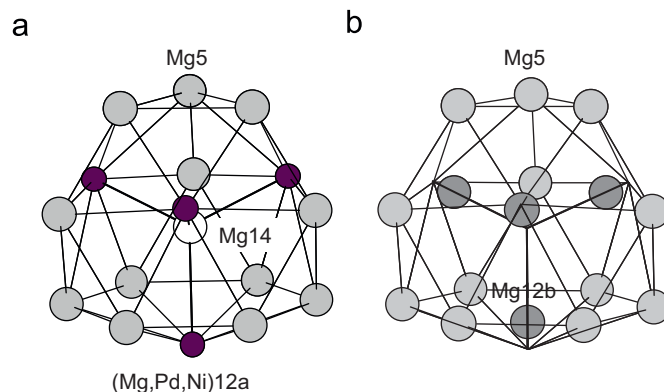**Fig. 1.** Coordination polyhedron around site Mg14 in pseudobinary $Mg_6(Pd,Ni)$ compounds. (a) Non-defective 16-vertex Frank Kasper polyhedron (Samson's model, [11]). (b) Point defects for Mg-rich compounds (Makongo's model [17]).

under consideration. The third equation was obtained from the crystallographic constraint $\Sigma(\mathrm{SOF}12a, \mathrm{SOF}12b) = 1$. The analytical SOF_M12a result was then introduced in the Fullprof program and the obtained SOF refined parameters for other sites were considered for analytical re-calculation of SOF_M12a values. This iterative process was followed for three times showing a very fast convergence. The final Rietveld refinement is shown in Fig. 2 and the results are gathered in Table 1. The end residuals of the refinement are: $R_B = 1.98\%$ and $R_{wp} = 1.75\%$. With the exception of the site 12b, the refined positional parameters and therefore the interatomic distances, are quite close to that reported by Samson for $\mathrm{Mg}_6\mathrm{Pd}$ compound [11]. The interatomic distance between sites 12b and 12a is very short, 0.68(2) Å and, of course, simultaneous atomic occupation on both sites is not possible. The structural model accounted for this circumstance by imposing that the SOF at both sites fulfill the equation $\Sigma(\mathrm{SOF}12a, \mathrm{SOF}12b) = 1$. As for the isotropic displacement factors, B, all take reasonable values except for site 14, $B_{14} = 3.25\,(70)\,\text{Å}^2$. The substitutional disorder on the

neighboring site 12a (see Fig. 1) may account for such a high value. The refined unit-cell composition is $\mathrm{Mg}_{342(1)}\mathrm{Pd}_{29(1)}\mathrm{Ni}_{23(1)}$ and the calculated crystal density is 2.60 g/cm^3, which is in good agreement with the pycnometric measurements (2.58 (1) g/cm^3). The formula unit (f.u.) of the compound can be described as $\mathrm{Mg}_{6.10(2)}\mathrm{Pd}_{0.52(2)}\mathrm{Ni}_{0.41(2)}$, leading to $Z = 56$ f.u. in the unit-cell.

Fig. 3 shows, for each crystallographic site, the percentage of nickel atoms that substitute palladium ones and its comparison with the statistical substitution according to the EPMA chemical analysis, 44(2) at% Ni for $\mathrm{Mg}_{86.7(2)}\mathrm{Pd}_{7.4(2)}\mathrm{Ni}_{5.9(3)}$ compound. Nickel preferentially replaces Pd at site 11, whereas it is almost absent at site 12a. A perfect statistical substitution occurs at site 13 and almost for site 10. This atomic distribution seems to be closely linked to the coordination number (CN) of each site. Ni atoms prefer the site with low CN (i.e., site 11), whereas Pd ones prefer the site with high CN (i.e., site 12a). This can be explained by the
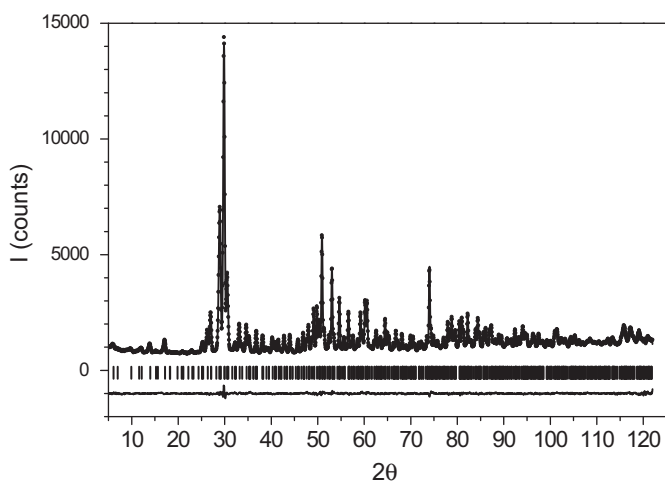

Fig. 2. Rietveld analysis of neutron powder diffraction data ($\lambda = 1.2243\,\text{Å}$) at room temperature for the pseudo-binary $\mathrm{Mg}_6\mathrm{Pd}_{0.5}\mathrm{Ni}_{0.5}$ compound.
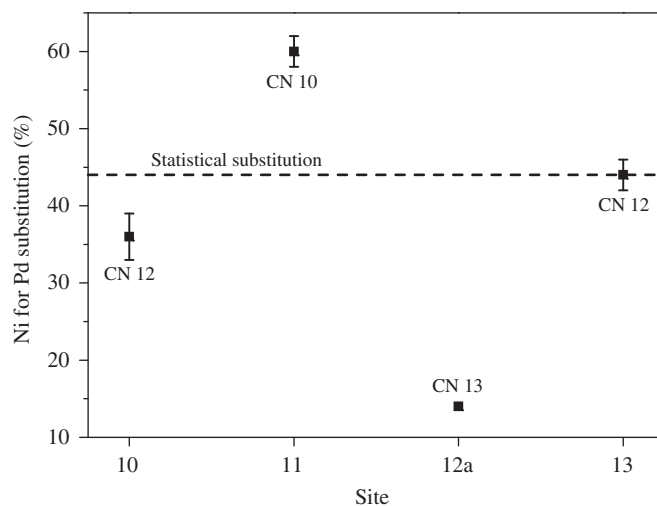

Fig. 3. Substitution of Pd by Ni atoms at different crystallographic sites for the pseudo-binary $\mathrm{Mg}_6\mathrm{Pd}_{0.5}\mathrm{Ni}_{0.5}$ compound. Coordination numbers (CN) of each site are expressly indicated.

Table 1
Structural parameters for the pseudo-binary $\mathrm{Mg}_6\mathrm{Pd}_{0.5}\mathrm{Ni}_{0.5}$ compound.

Site no.	Atom	Wyckoff	x	y	z	B (Å^2)	SOF
1	Mg	48(h)	0.1435(2)	x	0.0352 (3)	1.08(7)	1
2	Mg	48(h)	0.0947(2)	x	0.2750 (2)	1.06(7)	1
3	Mg	48(h)	0.1502(2)	x	0.5254 (3)	1.77(10)	1
4	Mg	48(h)	0.0559(2)	x	0.7678 (3)	1.18(8)	1
5	Mg	48(h)	0.1990(2)	x	0.9098 (3)	1.48(8)	1
6	Mg	24(f)	0.1065(3)	0	0	0.88(8)	1
7	Mg	24(f)	0.3827(3)	0	0	1.34(8)	1
8	Mg	24(g)	0.0659(4)	$\frac{1}{4}$	$\frac{1}{4}$	1.42(10)	1
9	Mg	16(e)	0.3023(2)	x	x	1.20(13)	1
10	Pd	16(e)	0.1680(2)	x	x	0.96(10)	0.64(3)
10	Ni						0.36(3)
11	Pd	16(e)	0.4069(1)	x	x	1.00(8)	0.40(2)
11	Ni						0.60(2)
12a	Pd	16(e)	0.6682(5)	x	x	1.61(17)	0.24[a]
12a	Ni						0.04[a]
12a	Mg						0.44[a]
12b	Mg	16(e)	0.6877(9)	x	x	1.61(17)	0.28(1)
13	Pd	16(e)	0.9003(1)	x	x	0.90(8)	0.56(2)
13	Ni						0.44(2)
14	Mg	4(d)	$\frac{1}{4}$	$\frac{1}{4}$	$\frac{3}{4}$	3.25(70)	0.72(5)

S.G. $F\bar{4}3m$, $a = 20.13331\,(7)$ Å; $R_B = 1.98\%$, $R_{wp} = 1.75\%$; $\chi^2 = 1.84$.
The standard deviations are given in parentheses.
No. independent reflections: 688. No. intensity variables: 37.

[a] SOF of site 12a analytically determined (see text for details).

larger atomic radius of Pd as compared to nickel ($r_{Pd} = 1.37$ Å, $r_{Ni} = 1.23$ Å). Large atoms preferentially locate at sites with high CN where more space is available to accommodate their size, as it has widely been reported for Frank-Kasper type phases [18].

3.2. Deuteration of $Mg_6Pd_{0.5}Ni_{0.5}$ compound

The intermetallic compound was deuterated by solid–gas reaction at 573 K. The PCI absorption curve is shown in Fig. 4. The compound absorbs up to 9.59 deuterium atoms by formula unit (D/f.u.) at 23 bar, which corresponds to a mass capacity of 7.77 wt% of deuterium in the deuterated sample. For comparison purposes, Fig. 4 displays the mass capacity in hydrogen units with a maximum content of 4.07 wt% H. Absorption occurs through a two-step plateau very close in pressure (Pp~2.5 bar) up to 3.2 wt% H, followed by a gradual increase of the equilibrium pressure with deuterium concentration.

PCI absorption curves for the binary Mg_6Pd compound have recently been reported by several authors. Yamada et al. [5] have observed at 523 K three plateau pressures on the PCI curve of $Mg_{89}Pd_{11}$ alloy. The alloy was found to be two-phase $Mg+Mg_6Pd$. Plateau pressures appeared at about 1, 1.5 and 15 bar of hydrogen pressure. They were attributed to the formation of magnesium hydride, MgH_2, the decomposition of Mg_6Pd phase into a mixture of Mg_5Pd_2 and MgH_2, and the formation of a hypothetical Mg_5Pd_2 hydride, respectively. The hydrogen mass capacity for the fully hydrided sample was $C = 4.8$ wt% H. Later, Takeichi et al. [7], using single phase Mg_6Pd specimens, reported quite similar isotherms at 573 K. The fully hydride sample, $C = 4.1$ wt% H, was obtained at 33 bar and it consisted of a mixture of MgPd and MgH_2 phases, proving that Mg_5Pd_2 phase disproportionates after hydrogen uptake. Furthermore, at low pressures (~2 bar) they mentioned the formation of an intermediate product. Very recently, Huot et al. [8] have confirmed the existence of three plateaus with pressure of about 4, 5 and 30 bars in the PCI curve of Mg_6Pd at 573 K. All of them were shown to be related to disproportionation reactions. They were attributed to the decomposition of Mg_6Pd into $Mg_{3.65}Pd$ and MgH_2, the decomposition of $Mg_{3.65}Pd$ into Mg_5Pd_2 and MgH_2, and the decomposition of Mg_5Pd_2 into MgPd and MgH_2, respectively. The hydrogen mass uptake was about 1.3, 1.4 and 1.6 wt% H for each three reactions, respectively, to sum up 4.3 wt% H for the fully hydrided sample.
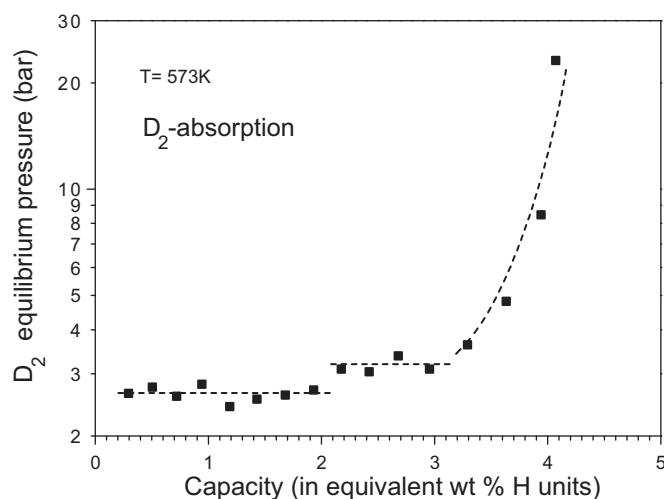

Fig. 4. PCI deuterium absorption isotherm at 573 K for the pseudo-binary $Mg_6Pd_{0.5}Ni_{0.5}$ compound. Capacity is given in equivalent wt% hydrogen units. Dashed lines are guides to the eye.

Based on these results for the binary alloy, the PCI curve for the pseudo-binary $Mg_6Pd_{0.5}Ni_{0.5}$ compound can tentatively be split into three parts as shown by dashed lines on Fig. 4. Two close plateau pressures at 2.6 and 3.2 bar occur for $C < 3.2$ wt% H, probably related to two distinct disproportionation reactions. No additional plateau was observed to occur up to 23 bar.

3.3. Structural study of $Mg_6Pd_{0.5}Ni_{0.5}$ compound after deuteration

After the acquisition of the above reported PCI curve, the sample was cooled down to room temperature and the deuterium pressure in the chamber was lowered to 1 bar. Deuterium uptake on cooling is almost negligible. The final deuterium concentration of the sample is 9.73 D/f.u. (7.87 wt% D). Its crystal structure was then studied by joint Rietveld analysis of NPD and XRPD data.

Fig. 5 shows the fit of the NPD and XRPD patterns. Main diffraction peaks can be indexed with three phases: MgD_2 (S.G $P4_2/mnm$), Mg_5Pd_2 (S.G. $P6_3/mmc$) and Mg_2NiD_4 (S.G. $Pcc2$). The abundance and crystallographic data of these phases are summarized in Table 2. Rietveld agreement factors are provided in Table 3. The main phase corresponds to magnesium deuteride with a phase abundance of 52(2) wt%. Crystallographic data for this phase are in close agreement with previous publications [19,20]. The second phase corresponds to the intermetallic compound Mg_5Pd_2 with a phase abundance of 29(2) wt%. The end-formation of Mg_5Pd_2 instead of MgPd as reported by several authors [7,8] is well explained by the fact that the disproportionation of Mg_5Pd_2 at 573 K occurs at a hydrogen pressure (~30 bar) higher than that used in our study (23 bar). Mg_5Pd_2 phase is found to crystallize in a hexagonal Co_2Al_5 type structure. The crystallographic data concur with a recent publication of Hlukhyy and Pöttgen [21]. In particular, the unit-cell volume of this phase (531.4(1) Å³) matches with that reported by the cited authors (531.6 Å³). This suggests that no significant solution of deuterium occurs in this phase. Furthermore, refinement of possible substitution of Pd by Ni in either $2c$ or $6h$ sites shows negative results. As for the third phase, it corresponds to Mg_2NiD_4 with a phase abundance of 18(2) wt%. The particular crystallographic properties of this phase, whose peaks have been indexed in the orthorhombic $Pcc2$ space group, deserve a more detailed discussion.

Mg_2NiH_4 exhibits rather complicated polymorphic properties [22–29]. At high temperature ($T > 508$ K) it crystallizes in a cubic high-temperature modification (HT) with S.G. $Fm\bar{3}m$. At low temperature ($T < 483$ K), a monoclinic modification (LT1) is obtained with S.G. $C2/c$. In addition, when Mg_2NiH_4 is prepared in the high temperature domain and cooled below the transition temperature, a second low temperature modification (LT2) with orthorhombic symmetry is partially obtained. As reported by Zolliker et al. [24], LT2 phase results from microtwining in the LT1 phase associated to the HT→LT phase transformation. The twining probability is usually lower than 50% and therefore the existence of a pure LT2 phase was discarded.

Taking into consideration the crystallographic properties of Mg_2NiH_4, the indexation of remaining peaks (i.e. besides those assigned to MgD_2 and Mg_5Pd_2 reflections) in the diffraction patterns of the deuterated sample was checked. For example, Fig. 6 shows the NPD pattern in the selected range $0.12 < \sin\theta/\lambda < 0.145$ Å⁻¹ in which the main diffraction lines of LT1 and LT2 modifications may appear. The diffraction data can be clearly indexed in the orthorhombic LT2 modification (($211)_O$ line at 0.1335 Å⁻¹) but not in the monoclinic LT1 one (($111)_M$ and $(-311)_M$ lines at 0.1310 and 0.1361 Å⁻¹, respectively). Furthermore, the absence of the characteristic double-peak feature of the LT1 phase in this acquisition domain suggests a very high probability of
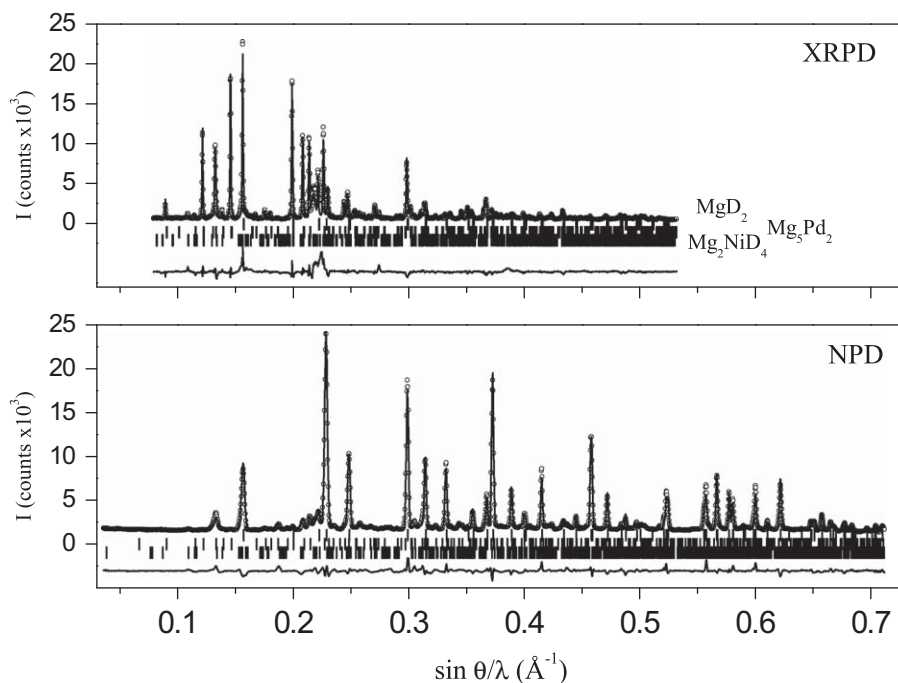
Fig. 5. Joint XRPD and NPD Rietveld analysis of $Mg_6Pd_{0.5}Ni_{0.5}$ compound after deuteration. Experimental data (circles), calculated diffraction patterns (continuous line), diffraction line positions (vertical bars) and difference curves at the same scale (below) are given.

Table 2
Phase content and structural parameters of $Mg_6Pd_{0.5}Ni_{0.5}$ sample after deuteration.

Phases	Atom	Site	x	y	z	B (Å^2)	SOF
MgD_2			Content: 52(2) wt%, S.G: $P4_2/mnm$, $a = 4.4992(1)$ Å, $c = 3.0101(1)$ Å, $V = 60.934(6)$ Å^3				
	Mg	2a	0	0	0	0.85(9)	1
	D	4f	0.3043(6)	x	0	1.54(6)	1
Mg_5Pd_2			Content: 29(2) wt%, S.G: $P6_3/mmc$, $a = 8.6677(9)$ Å, $c = 8.168(1)$ Å, $V = 531.4(1)$ Å^3				
	Pd1	2c	$\frac{1}{3}$	$\frac{2}{3}$	$\frac{1}{4}$	1.7(4)	1
	Pd2	6h	0.875(2)	2x	$\frac{1}{4}$	1.7(4)	1
	Mg1	2a	0	0	0	0.7(4)	1
	Mg2	6h	0.543(7)	2x	$\frac{1}{4}$	0.7(4)	1
	Mg3	12k	0.192(5)	2x	0.063(5)	0.7(4)	1
Mg_2NiD_4			Content: 18(2) wt%, S.G: $Pcc2$, $a = 13.10(1)$ Å, $b = 6.408(4)$ Å, $c = 6.470(4)$ Å, $V = 543.0(7)$ Å^3				
	Ni1	4e	0.1194	0.2308	0.9638	3.3(5)	1
	Ni2	4e	0.3806	0.7308	0.0362	3.3(5)	1
	Mg1	4e	0.2652	0.4827	0.8102	3.3(5)	1
	Mg2	4e	0.2348	0.9827	0.1898	3.3(5)	1
	Mg3	2a	0	0	$\frac{3}{4}$	3.3(5)	1
	Mg4	2d	$\frac{1}{2}$	$\frac{1}{2}$	$\frac{1}{4}$	3.3(5)	1
	Mg5	2b	0	$\frac{1}{2}$	$\frac{3}{4}$	3.3(5)	1
	Mg6	2c	$\frac{1}{2}$	0	$\frac{1}{4}$	3.3(5)	1
	D1	4e	0.2113	0.2995	0.0924	3.3(5)	1
	D2	4e	0.2887	0.7995	0.9076	3.3(5)	1
	D3	4e	0.1360	0.3163	0.7451	3.3(5)	1
	D4	4e	0.3640	0.8163	0.2549	3.3(5)	1
	D5	4e	0.0105	0.2868	0.0432	3.3(5)	1
	D6	4e	0.4895	0.7868	0.9568	3.3(5)	1
	D7	4e	0.1306	0.9950	0.9509	3.3(5)	1
	D8	4e	0.3694	0.4950	0.0491	3.3(5)	1

The standard deviations are given in parentheses.

twinning. The same picture applies for the analysis of XRPD data. The occurrence of the LT2 modification is expected from the fact that the sample was deuterated at 573 K, i.e. above the HT→LT phase transformation, and then cooled down to room temperature. In contrast, the absence of the LT1 modification is highly unexpected (see Ref. [24]) and is maybe due to the particular microstructure of the deuterated sample with the

formation of Mg_2NiD_4 precipitates in the sub-micrometric range [30].

In order to introduce the LT2 modification in the Rietveld analysis, we have considered the model proposed by Zolliker et al. [24] to infer the space group, cell parameters and atomic coordinates for this phase. In brief, Zolliker's model proposes that the LT2 structure is formed by twinning planes at $a/2$ which are

Table 3
Reliability factors of the conjoint PND/PXRD Rietveld refinement on deuterated $Mg_6Pd_{0.5}Ni_{0.5}$ sample.

	R_B (MgD_2) (%)	R_B (Mg_5Pd_2) (%)	R_B (Mg_2NiD_4) (%)	R_p (%)	R_{wp} (%)	χ^2
ND	5.9	15.0	21.9	3.89	5.45	31.4
XRD	16.2	10.7	20.2	9.81	14.5	25.0

No. independent reflections: 90. No. intensity variables: 9
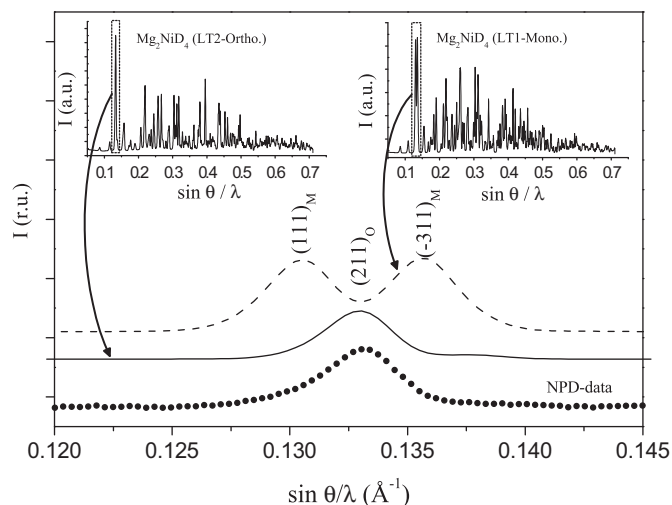
Fig. 6. Comparison of NPD pattern in the range $0.12 < \sin\theta/\lambda < 0.145$ of deuterated $Mg_6Pd_{0.5}Ni_{0.5}$ sample with simulated NPD patterns for LT2 (continuous line) and LT1 (dashed line) modifications of Mg_2NiD_4 phase. Insets show the simulated NPD patterns for LT2 (orthorhombic symmetry, S.G. $Pcc2$) and LT1 (monoclinic symmetry, S.G. $C2/c$) modifications. Crystal data for LT2 phase are provided in Table 2. Crystal data for LT1 phase are obtained from Ref. [25].

parallel to the (100) plane of the monoclinic LT1 phase. The unit-cell parameters of the orthorhombic LT2 phase can be then derived from the monoclinic LT1 phase as: $a_O = a_M \sin\beta_M$, $b_O = b_M$ and $c_O = c_M$. Using the crystallographic data for the LT1 phase [25], the unit-cell parameters of LT2 are: $a_O = 13.1514$ Å, $b_O = 6.4038$ Å and $c_O = 6.4830$ Å. The LT2 structure is then built by two slabs of thickness $(a_M \sin\beta_M)/2$, both having the same metal arrangement as for the monoclinic modification but with different orientations. Thus, the new atomic coordinates for the orthorhombic LT2 phase were calculated. Due to symmetry considerations, a small shift (< 0.015 coordinate units) for the y-coordinates of Mg-atoms in the original $4e$ sites was allowed. This makes possible the description of the LT2 phase in the $Pcc2$ space group with the atomic coordinates given in Table 2.

The quality of the Rietveld fitting as shown by visual inspection of Fig. 5 and numerical data given in Table 3 is reasonable when considering the multi-phase complexity of the deuterated sample. Main deficiencies have to be assigned to the fitting of the Mg_2NiD_4 phase ($R_B \sim 20\%$). One reason for this, as suggested by Noréus and Kihlborg [27], could be that the twinning mechanism is more complex than that proposed by Zolliker et al. Moreover, diffuse reflections which are mainly observed in the XRPD pattern in the range 0.218–0.228 Å^{-1} can indicate incomplete twinning effects. Nevertheless, the proposed LT2 structure has to be considered as an average one which allows for a first approximation to phase identification, refinement of lattice parameters and abundance. Unfortunately, the low amount of this phase in the sample (~ 18 wt%) and the large number of refinable intensity parameters (52 independent coordinates) do not allow full structural refinement. The obtained lattice parameters are $a = 13.10(1)$ Å,

$b = 6.408(4)$ Å and $c = 6.470(4)$ Å, i.e., very close to those derived by using the Zolliker's microtwinning model. Such close values also suggest that no significant substitution of Ni by Pd occurs in the Mg_2NiD_4 phase.

To summarize, the intermetallic compound disproportionates on deuterium absorption according to the following reaction:

$$Mg_{6.1}Pd_{0.52}Ni_{0.41} + \frac{9.6}{2}D_2 \rightarrow 3.98MgD_2 + 0.26Mg_5Pd_2 + 0.41Mg_2NiD_4$$
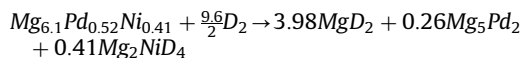
Neither Ni substitutes Pd in the Mg_5Pd_2 phase nor Pd substitutes Ni in the Mg_2NiD_4 phase. It is worth noting that the chemical composition of the intermetallic compound, as determined by EPMA, can be considered for the evaluation of deuterium uptake and phase abundances. According to this reaction, the deuterium uptake is 7.78 wt% D and matches well the quantity determined by solid–gas measurements (7.87 wt% D). The phase abundance derived from the disproportionation reaction is 45.6 wt% of MgD_2, 35.2 wt% of Mg_5Pd_2 and 19.1 wt% of Mg_2NiD_4. These values are in reasonable agreement with diffraction analysis (52(2), 29(2) and 18(2) wt% for MgD_2, Mg_5Pd_2 and Mg_2NiD_4 phases, respectively) after considering the quality of the refinement.

4. Conclusion

Single phase $Mg_{6.10(2)}Pd_{0.52(2)}Ni_{0.41(2)}$ intermetallic compound was obtained by induction melting as a stable phase. This compound is isotructural to Mg_6Pd. It crystallizes in $F\bar{4}3m$ space group with lattice parameter 20.13331(7) Å. Nickel atoms substitute Pd ones with a slight preference for crystallographic sites having low coordination number due to steric considerations.

Upon deuterium absorption at 573 K and 23 bar, the intermetallic compound disproportionates into MgD_2, Mg_5Pd_2 and Mg_2NiD_4 phases. This corresponds to a deuterium content of 7.77 wt% (i.e., 4.07 wt% H). Substitution of either Ni by Pd or *vice versa* in the end-products is not observed. Nevertheless, the disproportionation reaction is reversible with hydrogen pressure as shown in a forthcoming publication [30].

As a particular feature in the crystallography of the end-products, the Mg_2NiD_4 phase is observed to crystallize in the orthorhombic LT2 modification. Strikingly, contribution of LT1 modification to NPD and XRPD diffraction patterns is almost negligible. An average crystal structure of this phase with space group $Pcc2$ is proposed on the basis of the Zolliker's model for microtwinning in Mg_2NiD_4.

Appendix A. Supplementary material

Supplementary data associated with this article can be found in the online version at 10.1016/j.jssc.2009.07.049.

References

[1] R. Wiswall, in: G. Alefeld, J. Völkl (Eds.), Hydrogen in Metals II, Topics in Applied Physics, vol. 4, Springer, Berlin, Heidelberg, New York, 1978, pp. 201–242.

[2] J.J. Reilly, R.H. Wiswall, Inorg. Chem. 7 (1968) 2254–2256.
[3] B. Baranowsky, in: G. Alefeld, J. Völkl (Eds.), Hydrogen in Metals II, Topics in Applied Physics, vol. 4, Springer, Berlin, Heidelberg, New York, 1988, pp. 157–200.
[4] Y. Kume, A. Weiss, J. Less-Common Met. 136 (1987) 51–54.
[5] T. Yamada, J. Yin, K. Tanaka, Mater. Trans. 42 (2001) 2415–2421.
[6] C. Zlotea, Y. Andersson, Acta Mater. 54 (2006) 5559–5564.
[7] N. Takeichi, K. Tanaka, H. Tanaka, T.T. Ueda, Y. Kamiya, M. Tsukahara, H. Miyamura, S. Kikuvhi, J. Alloys Compd. 446–447 (2007) 543–548.
[8] J. Huot, A. Yonkeu, J. Dufour, J. Alloys Compd. 475 (2009) 168–172.
[9] H. Frieske, E. Wicke, Ber. Bunsenges. Phys. Chem. 77 (1973) 48–52.
[10] K.P. Gupta, J. Phase Equilib. Diffus. 25 (2004) 191–194.
[11] S. Samson, Acta Crystallogr. B28 (1972) 936–945.
[12] A. Teresiak, M. Uhlemann, J. Thomas, A. Gebert, J. Alloys Compd. 475 (2009) 191–197.
[13] S. Todorova, T. Spassov, J. Alloys Compd. 469 (2009) 193–196.
[14] A. Kamegawa, Y. Goto, R. Kataoka, H. Takamura, M. Okada, Renewable Energy 33 (2008) 221–225.
[15] J.F. Fernández, F. Cuevas, F. Leardini, J. Bodega, J.R. Ares, G. Garcés, P. Pérez, C. Sánchez, J. Alloys Compd. (2009), submitted for publication.
[16] J. Rodríguez-Carvajal, Physica B 192 (1993) 55–69.
[17] J.P.A. Makongo, Y. Prots, U. Burkhardt, R. Niewa, C. Kudla, G. Kreiner, Philos. Mag. 86 (2006) 427–433.
[18] J.-M. Joubert, Prog. Mater. Sci. 53 (2008) 528–583.
[19] W.H. Zachariasen, C.E.J. Holley, J.F.J. Stamer, Acta Crystallogr. 16 (1963) 352–353.
[20] M. Bortz, B. Bertheville, G. Böttger, K. Yvon, J. Alloys Compd. 287 (1999) L4–L6.
[21] V. Hlukhyy, R. Pöttgen, Intermetallics 12 (2004) 533–537.
[22] Z. Gavra, M.H. Mintz, G. Kimmel, Z. Hadari, Inorg. Chem. 18 (1979) 3595–3597.
[23] D. Noréus, P.-E. Werner, J. Less-Common Met. 97 (1984) 215–222.
[24] P. Zolliker, K. Yvon, C. Baerlocher, J. Less-Common Met. 115 (1986) 65–78.
[25] P. Zolliker, K. Yvon, J.D. Jorgensen, F.J. Rotella, Inorg. Chem. 25 (1986) 3590–3593.
[26] P. Zolliker, K. Yvon, Mater. Res. Bull. 21 (1986) 415–419.
[27] D. Noréus, L. Kihlborg, J. Less-Common Met. 123 (1986) 233–239.
[28] U. Häussermann, H. Blomqvist, D. Noréus, Inorg. Chem. 41 (2002) 3684–3692.
[29] J.F. Herbst, L.G. Hector, Phys. Rev. B 79 (2009) 155113–155119.
[30] J.F. Fernández, J.R. Ares, F. Cuevas, J. Bodega, F. Leardini, C. Sánchez, Intermetallics (2009), accepted for publication.